Shading Illusion : A Novel Way for 3-D Representation on Paper Media

Toshiyuki Amano
Department of Mechanical Systems Engineering
Graduate School of Science and Engineering, Yamagata University, Japan
amano@yz.yamagata-u.ac.jp

Abstract

Content printed on the paper media is not rewritable, but its appearances can be controlled by illumination. In this paper, we propose a new method to represent three-dimensional (3-D) shape on the print media by the shading animation using projector-camera feedback. The proposed method consists of a hue, saturation, and value (HSV) map and an appearance control technique, and these are key technologies. The HSV map represents a normal map of the 3-D content, and it is embedded in the printed media by full color print. While the system is projecting a shading animation for the 3-D representation, the embedded information is decoded by modulation estimation using the appearance control technique.

1. Introduction

The cues that allow us perceive the three-dimensional (3-D) world are broadly divided into binocular and monocular cues. In the early 19th century, the Anaglyph [14] that is the most primitive binocular parallax technique has been proposed and it remains dominant for 3-D representation (e.g. 3-D displays that requires LCD shutter glasses). However, the monocular cues of occlusion, shading, perspective, and motion parallax can provide a natural 3-D perception. This paper focuses on the shading cue and proposes a novel method of 3-D representation by animated shading on paper media using projector-camera feedback.

Newspapers, books, and the other printed materials are not rewritable naturally. However, their appearance can be determined by the relationship between modulation of the media and an illumination from the environment. Thus, the appearance can be changed by projection and with precisely controlled illumination one can change the shading on the printed 3-D contents. Besides appearance control, the printed media can be a new media that can give us a 3-D representation if it can retain 3-D information of the printed content in full color printing. The concept of our novel 3-D representation shown in Figure 1, is as follows:

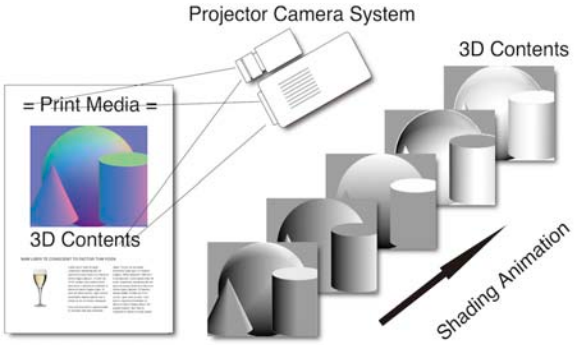

Figure 1. 3-D representation concept using shading animation.

- The 3-D shape is expressed by a normal map and is embedded in a paper media by full color printing.
- The normal map is reconstructed by color compensation and conversion of a captured image.
- The normal map is used to obtain a shading image, giving a reference for the projector-camera feedback.
- The appearance control technique changes the shading on the 3-D content.
- Shading animation using virtual light source motion provides a richer 3-D perception.

Shading and motion parallax are monocular cues and do not require the use of 3-D glass to view. This is an advantage of the proposed method. However, it does not preclude the use of binocular cues and two methods can complement.

The main contribution of this paper is the creation of a novel media that combines coded printing and a projector camera system. Dynamic shading control by precisely calculated illumination written on the paper is a first attempt, and it allows for a 3-D representation on paper media by a whole new approach. Another contribution is the development of a robust 3-D information embedding technique to enable illumination variation of the captured image. The advantage of this embedding is not limited to its robustness;

978-1-4673-1612-5/12/$31.00 ©2012 IEEE

it also provides us with an appearance compatible with a normal picture under unique white illumination.

2. Related Work

In the earliest work on appearance control, Nayar et al. [13] and Grossberg et al. [12] showed the capability of the appearance control using illumination projection. In later work, Fujii et al. [10] applied this irradiation compensation technique in dynamic scenes using a coaxial device configuration. Irradiation compensation was also implemented with smart calibration [5], and obtaining views of the human perception were also attempted [4]. Those works are very impressive and demonstrate the capability of controlling the shading of the printed 3-D content.

Different from irradiance compensation, appearance control techniques can enhance, change, and replace the visible appearance according to the original appearance of the projection target. The superimposed dynamic range technique proposed by Bimber et al. [7], allowed a high dynamic range display, and color compensation on the printed media by illumination projection. Amano et al. proposed a projector-camera feedback framework [2] that enables not only color saturation enhancement, and contrast boost but also color phase shift, posterlization and bluring [3] in a dynamical process. The appearance control technique is not limited to printed media and has been applied to light microscopy as well [6, 8]. Its technique enables the targets' appearance to look different, but its control is based on the reflectance property of the target. The projector-camera feedback in [8, 3] can estimate appearance under white unique illumination while a colored textured pattern is projected. This technique not only gives a good reference image for feedback control but also enables to receive 3-D information to be embedded by full color printing on the paper media.

The proposed method is also related to the mesostructure design technique for object representation written in [15, 1]. Both are brilliant ideas to show an image by the illumination projection. [1] employs a discrete relief model with a precisely designed relief shape, then it represents a different image using a different illumination direction. It has the ability to represent attached shadow of a 3-D object on a nearly planar media. However, the content manufacturing cost is still too expensive for use in the actual publishing.

In this research, the appearance control framework shown in Figure 2 is employed. First, the underlying appearance C_{est} which means the appearance that observed under the white uniform illumination is calculated with the division of captured image C by the projection pattern P. This C_{est} is invariant for P, and the reference image R is calculated by user defined image processing algorithm. Then, the appearance control framework changes the object's appearance by the projection after the geometric warp

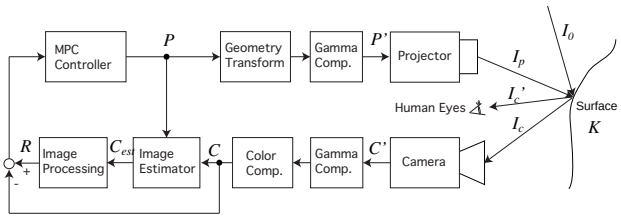

Figure 2. Projector-camera feedback with an MPC controller.

and response linearization. The proposed method attempts to control the shading by the decoded information of embedded in the full color printing.

3. 3-D Information Embedding

3.1. The Normal Map Image

In general computer graphic, a the rough shape is described by a sparse polygon mesh and the remaining details are expressed by a normal map image [9]. With this normal map image, we can embed 3-D information by a color printing. Its advantage is not only embedding, but also the special recognition algorithm is not required for 3-D information reconstruction. Thus, this research employs a normal map image for shape information embedding.

For the embedding, the normal vector on the 3-D content is projected on the $x-y$ plane as

$$\mathbf{n}(x,y) = (n_x(x,y), n_y(x,y), n_z(x,y)), \tag{1}$$

and it expressed by the color image

$$Sn(x,y) = (Sn_R, Sn_G, Sn_B), \tag{2}$$

$$\begin{cases} Sn_R(x,y) &= (n_x(x,y)+1)/2 \\ Sn_G(x,y) &= (n_y(x,y)+1)/2 \\ Sn_B(x,y) &= (n_z(x,y)+1)/2 \end{cases} \tag{3}$$

where $|\mathbf{n}(x,y)| = 1, 0 \leq Sn_i(x,y) \leq 1, i \in \{R,G,B\}$. Thus, the normal vector expressed in the color image is easily recovered by

$$\begin{cases} n_x(x,y) = 2Sn_R(x,y) - 1 \\ n_y(x,y) = 2Sn_G(x,y) - 1 \\ n_z(x,y) = 2Sn_B(x,y) - 1 \end{cases} . \tag{4}$$

However this encoding is not robust for illumination gain.

3.2. HSV Color Space Encoding

Since the projection pattern and captured image are obtained in the process, we can estimate the appearance C_{est} from white illumination irradiating the target, as shown in Figure 2. However, C_{est} is calculated as a relative luminosity with the reflectance standard (e.g., white paper) that used in the calibration. For this reason, it is impossible to

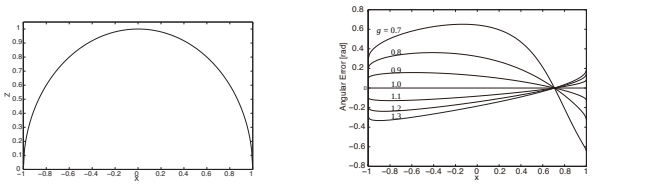

(a) Evaluation shape (b) Normal vector estimation error

Figure 3. Normal vector decoding error.

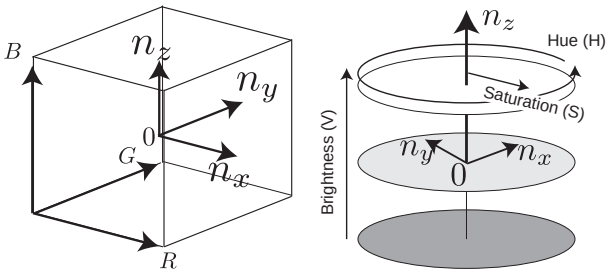

(a) Conventional (b) Proposed

Figure 4. Normal map expression on HSV space.

recover absolute image values, and this leads to a critical problem because the normal vector direction is sensitive to the gain of the normal map image.

On the cross section of sphere shown in figure 3(a), the decoded angular error of the normal vector led by the illumination gain variation is shown in Figure 3(b). The horizontal axis in (a) and (b) is spatial coordinate x, and the vertical axes are depth value z and angular error of the estimated normal vector, respectively. g is the gain of the received normal map image $S\mathbf{n}' = g \times S\mathbf{n}$. From this result, we can confirm that if the error in the estimated image is only 10%, then this leads to a 0.18 rad angular error in the estimated normal vector in the worst case.

To solve this problem, the HSV color space as an invariant expression

$$\begin{cases} Sn_H(x,y) &= atan2(n_y(x,y), n_x(x,y)) \\ Sn_S(x,y) &= k_s\sqrt{n_x(x,y)^2 + n_y(x,y)^2} \\ Sn_V(x,y) &= (n_z(x,y)+1)/2 \end{cases} \quad (5)$$

which is not influenced by illumination gain [1] (refer to as an HSV map), is used (Figure 4). The $atan2(y,x)$ is a general arctangent expression in a programing language that can handle four quadrants. The parameter k_s adjusts the contrast of the coded color image, and it should be decided by a tradeoff between controllability and stability. High-contrast embedding can transmit 3-D information precisely, but appearance control is difficult using projected illumination.

[1] The n_z is influenced, but we can recover it with a simple calculation.

In this normal vector coding, n_x and n_y are invariant for the illumination change of Sn. By contrast, n_z is influenced by the gain of Sn, but the constraint of $|\mathbf{n}(\mathbf{x},\mathbf{y})| = 1$ gives us the solution

$$n_z(x,y) = 1 - \sqrt{n_x(x,y)^2 + n_y(x,y)^2}. \quad (6)$$

Of course, its constraint gives the solution of g in the Figure 3. However, since a nonwhite color is expressed as $\mathbf{n}(x,y) = (0,0,1)$, which is perpendicular to the $x-y$ plane. Thus, nonlinear toner density response leads to an unbalanced reconstruction error by the (Sn_R, Sn_G, Sn_B) expression.

3.3. Normal Vector Decoding

The HSV map expression gives a neutral point for the normal map coding against paper brightness, and it gives a natural appearance. However, the printer color space and camera color space are not identical. This means that the color of the captured image is different from the color of the original HSV map image, leading to a decoding error of the normal vector. Therefore, a color mixing matrix $T_{c2s} \in \mathbf{R}^{3\times3}$ is applied to the captured image C_{est} as

$$S_{RGB} = T_{c2s} C_{est}, \quad (7)$$

where S_{RGB} is an HSV map image in RGB color space. $T_{c2s} \in \mathbf{R}^{3\times3}$ is a precalibrated color mixing matrix that is obtained by capturing the printed color chart. After color compensation, the RGB to HSV conversion is applied to get the S_{HSV} image. In this image, each channel corresponds to (Sn_H, Sn_S, Sn_V) and the normal vector can be recovered by

$$\begin{cases} n_x(x,y) = \frac{1}{k_s} Sn_S(x,y)\cos(Sn_H(x,y)) \\ n_y(x,y) = \frac{1}{k_s} Sn_S(x,y)\sin(Sn_H(x,y)) \\ n_z(x,y) = 2Sn_B(x,y) - 1 \end{cases} \quad (8)$$

and the normalization shown in Equation 6 is applied to n_z. Then, the shaded image used as reference R for appearance control is generated based on this normal map image and the virtual illumination by the graphics hardware.

4. Experimental Results

4.1. System Calibration

The desktop projector camera system shown in the Figure 5 was used in the experiment. This system is composed of a projector (Canon, LV-7380) and an IEEE1394 camera (Point Gray Research, Dragon Fly2) with two surface reflection mirrors. The alignment of the camera and the projector is almost colinear but the working space for the projector-camera feedback is limited on the desk surface to keep static pixel mapping. On the colinear (more

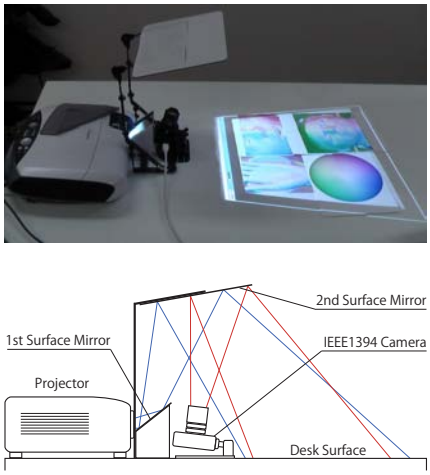

Figure 5. Desktop projector-camera system.

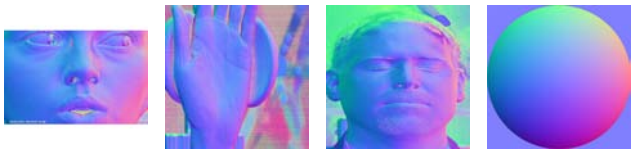

(a) Face1 (b) Hand (c) Face2 (d) Sphere

Figure 6. The normal map images.

(a) Face1 (b) Hand (c) Face2 (d) Sphere

Figure 7. HSV map images.

correctly, exit pupils are coaligned) projector-camera system, we can apply projector-camera feedback at any depth that has focus [10]. A general pixel mapping calibration that employed gray code projection is used for system calibration. Then, a system response linearization that includes both camera gamma and projector illumination response is applied. Next, the color-mixing matrix calibration for the projector-camera feedback and the gain-table calculation for photometric calibration shown in [3] were applied.

For color matching between a captured printed media C_{patt} and a digital image S_{patt}, the optimization problem on

$$Error = \sum_{i \in \{I_1, I_2, \ldots, I_n\}} (S^i_{patt} - T_{c2s} C^i_{patt}) \qquad (9)$$

is solved by capturing the printed color chart. $I_1, I_2, \ldots, I_n$ are the indices of the sampled colors (3×6 colors + 6 gray levels) and each sample is obtained by regional averaging. The pattern is printed on white matte photo paper using an inkjet printer (Canon, PIXUS MP960). Its appearance is then captured by the projector-camera system under white illumination. The matrix $T_{c2s} \in \mathbb{R}^{3\times3}$ is the color-mixing matrix, and it compensates for the chromatic characteristics of the inkjet printer.

4.2. HSV Map Conversion

Figure 6 shows the normal map images used for the evaluation. These are provided by the Digital Emily project (a), Face Dataset (b), and Palm Dataset (c) of the Graphics Lab at the University Southern California (USC) [11]. (d) is a artificial normal map image of the hemisphere. The HSV map images for these are shown in Figure 7. Parameter $k_s = 0.5$ was decided upon in consideration of the appearance controllability and the sensing stability from the experiment.

In these HSV map images, the center part that has $\mathbf{n} \approx (0, 0, 1)$ becomes white in the encoded images. Generally, when a sphere or cylinder is uniformly illuminated from the front, the center part shows a bright reflection for its attached shadow. The normal vector expression by the HSV map shows a similar tendency and it gives compatible appearance under white uniform illumination. This is another advantage of the HSV map expression.

4.3. Shading Control Details

When colored illumination is projected onto the printed target for shading control, the dumped images of the intermediate process shown in figure 8 were obtained. (a) is an underlying appearance that is not influenced by the projection, and it is calculated by the appearance control framework. The HSV map image shown in (b) can be obtained by color space conversion T_{c2s} and it converts the HSV map to the conventional normal map image (c). During this conversion, normalization by the Equation 6 is applied. Then, the shaded image (d) is generated by conventional normal map image rendering on the rendering hardware. However, I_{shade} has extremely high contrast, which leads to an unstable response because division by near zero arose at the complete black projection. Hence, mixing with the gray-scaled C_{est},

$$R = \alpha I_{shade} + (1 - \alpha)|C_{est}| \qquad (10)$$

is applied to avoid this problem. Here $|C_{est}|$ is gray-scaled C_{est}, and α is a mixing parameter. For this paper, $\alpha = 0.6$ was applied experimentally.

When reference R shown in (e) is given to the appearance control framework, the image P shown in (f) was projected onto the target object, and the appearance of the 3-D content on the paper was changed as shown in (g). In this case, a virtual point light source was placed on the upper right of the target and the correct directional shading based on the normal map information and its illumination is confirmable in (g). It is apparently different from the simple

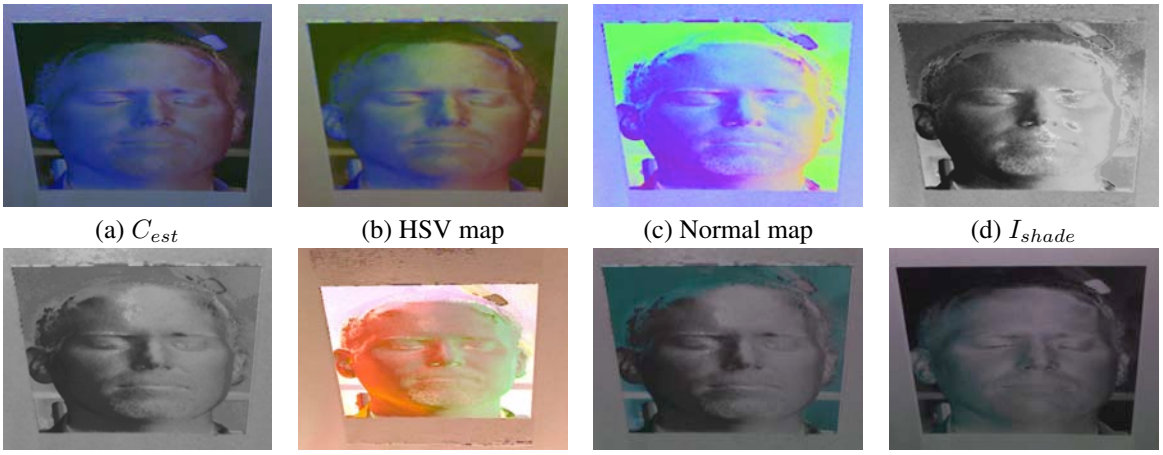

(a) C_{est} (b) HSV map (c) Normal map (d) I_{shade}

(e) R (f) P (g) Shading control (h) Color removal

Figure 8. Normal map reconstruction and appearance control.

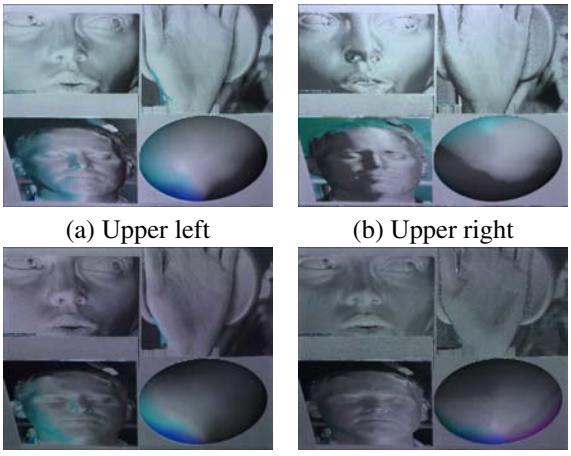

(a) Upper left (b) Upper right

(c) Lower left (d) Lower right

Figure 9. Shading with different illumination direction.

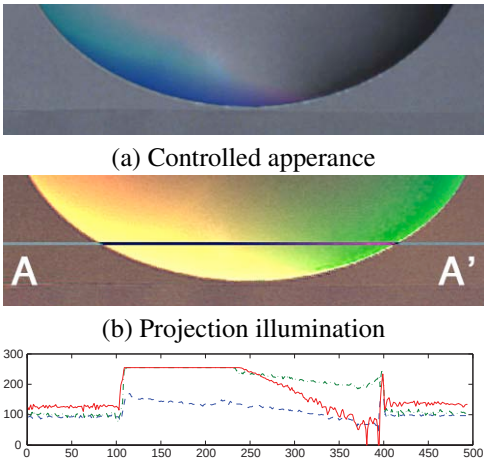

(a) Controlled apperance

(b) Projection illumination

(c) Illumination profile on the A-A'

Figure 10. Fake blue shadow.

color removal shown in (h). The proposed method was implemented on an Apple Mac Pro (with 12 cores and 8GB of memory) and its processing speed reached 19 fps with parallel computing with 1024×768 resolution of C and P.

4.4. Shading Animation

To promote effective 3-D perception to the user, shading animation by moving virtual illumination was implemented. A virtual point light source revolved on the 3D contents at 0.2 rad/frame. Thus, the light source moves at approximately 1.65 cycle/s.

Figure 9 shows the shading control results for the four illumination directions. In Figure 9 (a), when the virtual point light source is placed on the upper left of the paper media, the attached shadows can be seen at the counter side of each 3-D content. From the result for the different virtual light source positions, reasonable shading directions can be seen on the spheres. However, awkward-shaped shading was observed on the sphere in (c), and a fake blue shadow is seen in the left lower part on the sphere and the face image.

5. Discussion

5.1. Overprojection

The main factor contributing to the fake blue shadow can be thought of as insufficient projection power. Figure 10 shows the projection power profile on the fake blue shadow. In (c), the saturation of the projection power can be seen. This saturation means that there was insufficient power to fill the brightness in R and G channels, resulting in the blue-colored shading. Thus, we can expect that a more powerful projector can create the correct gray shadows.

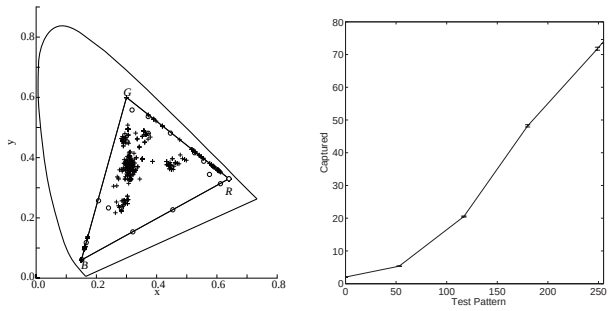

(a) Chroma chart (b) Brightness response

Figure 11. Color gamut and brightness response

5.2. Printer Color Space

Since the color in the normal map determines the direction of the surface normal, the color-matching error between the digital image and a captured printed image can be a main factor contributing to awkward-shaped shading. Figure 11 (a) shows the color distribution of the test pattern ("Circle") and its captured color ("Cross") on the x-y chroma chart. We can confirm good correspondence in the center areas, but the pure red and pure green areas have no plot. From this result, we can expect that a large normal estimation error can be seen in the pure green and pure red areas on the printed HSV map. This trend can be confirmed using the result from the sphere shown in Figure 9 (c). The nonlinearity of printed toner density is considered as the main reason leading to this color-matching error.

The figure 11(b) shows the brightness relationship between the test pattern and the captured image. A nonlinear response can be seen in the dark part, and it is easy to see that a linear model expression of this response produces a color conversion error at the dark part (around 50 to 150 in the test pattern). Since the pure red (or pure green) color has a big value at the R (or G) channel but others have small values, these color phases have large estimation errors. Hence, because of these large errors in these color phases, we can see the awkward-shaped shading in the pure red and pure green areas. The solution to this problem involves improvement of the color matching with response linearization. However, the linearization should not be applied to the captured image, and it should be applied before printing to ensure color invariance for different of paper whiteness.

6. Conclusion

In this paper, a new approach for 3-D representation on printed media was proposed. The proposed method consists of information embedding using an HSV map and shading animation using projector-camera feedback. This is a first attempt at 3-D representation on paper media by shading animation of the content. In the future work, improved color consistency between the normal map image and the captured printed image by using a predesigned print will be applied.

References

[1] M. Alexa and W. Matusik. Reliefs as images. *ACM Trans. Graph.*, 29:60:1–60:7, July 2010. 2

[2] T. Amano and H. Kato. Real world dynamic appearance enhancement with procam feedback. In *Proc. of the 5th ACM/IEEE International Workshop on Projector camera systems*, pages 1–2, 2008. 2

[3] T. Amano and H. Kato. Appearance control using projection with model predictive control. In *Proc. of International Conference on Pattern Recognition*, pages 2832–2835, Los Alamitos, CA, USA, 2010. IEEE Computer Society. 2, 4

[4] M. Ashdown, T. Okabe, I. Sato, and Y. Sato. Robust content-dependent photometric projector compensation. In *Proceedings of the 2006 Conference on Computer Vision and Pattern Recognition Workshop*, CVPRW '06, pages 6–, Washington, DC, USA, 2006. IEEE Computer Society. 2

[5] O. Bimber, A. Emmerling, and T. Klemmer. Embedded entertainment with smart projectors. *Computer*, 38:48–55, 2005. 2

[6] O. Bimber, A. Grundhöfer, D. Kurz, S. Thiele, F. Häntsch, T. Amano, and D. Klöck. Projected light microscopy. In *SIGGRAPH 2009: Talks*, pages 1–1, 2009. 2

[7] O. Bimber and D. Iwai. Superimposing dynamic range. *ACM Trans. Graph.*, 27(5):150:1–150:8, Dec. 2008. 2

[8] O. Bimber, D. Klöck, T. Amano, A. Grundhöfer, and D. Kurz. Closed-loop feedback illumination for optical inverse tone-mapping in light microscopy. *IEEE Trans. on Visualization and Computer Graphics*, 17:857–870, 2011. 2

[9] P. Cignoni, C. Montani, C. Rocchini, and R. Scopigno. A general method for preserving attribute values on simplified meshes, 1998. 2

[10] K. Fujii, M. D. Grossberg, and S. K. Nayar. A projector-camera system with real-time photometric adaptation for dynamic environments. In *Proc. of the Computer Vision and Pattern Recognition - Volume 2*, page 1180, 2005. 2, 4

[11] Graphics Lab. University Southern California, Face and Palm Dataset. http://gl.ict.usc.edu/Research/FaceScanning/. 4

[12] M. D. Grossberg, H. Peri, S. K. Nayar, and P. N. Belhumeur. Making one object look like another: Controlling appearance using a projector-camera system. *Computer Vision and Pattern Recognition, IEEE Computer Society Conference on*, 1:452–459, 2004. 2

[13] S. K. Nayar, H. Peri, M. D. Grossberg, and P. N. Belhumeur. A projection system with radiometric compensation for screen imperfections. In *IEEE International Workshop on Projector-CameraSystems*, 2003. 2

[14] W. Rollmann. Zwei neue stereoskopische methoden. *Annalen der Physik*, 166(9):186–187, 1853. 1

[15] T. Weyrich, P. Peers, W. Matusik, and S. Rusinkiewicz. Fabricating microgeometry for custom surface reflectance. *ACM Trans. Graph.*, 28(3):32:1–32:6, July 2009. 2